SPATIAL AND TEMPORAL TRENDS IN MUNICIPAL WATER INPUTS TO AN URBAN HEADWATER CATCHMENT

Camille E. Buckley, B.S.

A Thesis Presented to the Graduate Faculty of
Saint Louis University in Partial Fulfillment
of the Requirements for the Degree of
Master of Science

2020

COMMITTEE IN CHARGE OF CANDIDACY:

Associate Professor Elizabeth Hasenmueller,
Chairperson and Advisor

Professor Craig Adams

Professor Jason Knouft

ACKNOWLEDGEMENTS

This work was funded by a research grant from the Litzsinger Road Ecology Center (LREC) and other funds from Saint Louis University. The ICP-OES data for this study were collected on a PerkinElmer Optima 8300 funded by the National Science Foundation (CHE-1626501) and Saint Louis University. Thank you to Teresa Baraza Piazuelo, Carly Finegan, Abby Ritter, Maria Sakowski, Ashleigh Montgomery, Thomas Iborg, Mary O'Connell, Calvin Higgins, Ethan Wetter, and Katie Cassidy for their help with lab and field work and support throughout the last two years. Thank you to Teresa Baraza Piazuelo and Rio Febrian for assistance with the IC and ICP-OES. Thank you to Evan Montgomery and Jim Hessel at the Metropolitan St. Louis Sewer District (MSD) for respectively providing wastewater infrastructure data and wastewater samples and to LREC for allowing access to the property for sampling. I'd like to thank my committee members, Dr. Craig Adams and Dr. Jason Knouft for their input and support. Special thanks and gratitude go out to my advisor Dr. Elizabeth Hasenmueller for her guidance throughout this journey and for giving me the opportunity to grow and learn. Finally, thank you to my family and my mom who have supported me and my education for the last 25 years; I wouldn't be here without you.

TABLE OF CONTENTS

LIST OF TABLES

LIST OF FIGURES

CHAPTER 1: INTRODUCTION

As populations around the world grow, 68% of people are projected to live in urban areas by 2050 (United Nations, 2018). This urban expansion increases the demand for drinking water and the production of wastewater, potentially modifying water quantity and reducing water quality. Drinking water can enter urban streams through the irrigation of lawns or due to leaks from pressurized pipes. Wastewaters can be released to streams through discharges of treated effluent from wastewater treatment plants, overflows of untreated wastewater through combined sewer overflows (CSOs) and sanitary sewer overflows (SSOs), or leaks from infrastructure. Wastewater discharges can contaminate surface water and groundwater with harmful bacteria (*E. coli*), emerging contaminants (personal care products, pharmaceuticals, and microplastics), excess nutrients, and toxic metals.

In the United States alone, almost 34 billion liters of drinking water are used every day for outdoor water needs (USEPA, 2019a). These outdoor water uses can introduce drinking water to streams directly through surface runoff or indirectly through infiltration, the recharge of groundwater, and then groundwater contributions to streams through baseflow (Rugel et al., 2016; Keefe et al., 2019). Drinking water can also be introduced to streams from leaks in pressurized pipes. The pressurization of pipes inhibits the contamination of drinking water by groundwater, but leads to exfiltration of drinking water into the subsurface through cracks in the pipes. One large concern regarding drinking water infrastructure is age, since failures in pipes increase as the infrastructure ages. Aging infrastructure, therefore, leads to larger contributions of drinking water to the subsurface. Overall, around 14-18% of drinking water is lost through leaking pipes, and nearly 240,000 water main breaks occur every year, resulting in 23 million

liters of water lost every day (ASCE, 2018). These large contributions of drinking water have been found to make up to 54% of streamflow in urban environments (Lockmiller et al., 2019).

Wastewater treatment plants (WTPs) treat 129 billion liters of wastewater every day in the United States (USEPA, 2019b). On the way to WTPs, untreated wastewater can reach streams through CSOs, SSOs, and leaking pipes. The CSOs and SSOs typically discharge untreated wastewaters during high precipitation events when sewer systems are overwhelmed or as the result of backed up pipes (USEPA, 2018). Leaks in sewer pipes can occur due to the pipes reaching or exceeding their lifespan of 80-100 years (ASCE, 2011), as seen in many major cities in the United States. Leaking pipes contribute an estimated 3.41 trillion liters of untreated sewage to the environment every year due to aging sewage infrastructure (ASCE, 2019). These failures lead to the exfiltration of wastewater, which contributes untreated wastewater to the subsurface.

The presence of drinking water and wastewater in natural waterbodies can be detected using chemical tracers (such as B, F^-, and optical brighteners (OBs)). These tracers are present in high amounts within the municipal water sources compared to stream background levels due to their additions during water use (Pfeiffer et al., 2008; USDH, 2015; Lockmiller et al., 2019). In particular, F^- can be used to trace drinking water, B can be used to trace wastewater, and OBs can be used to trace wastewater.

Fluoridation of drinking water is prevalent in many areas worldwide to improve dental hygiene. In the United States, 66.3% of the population receives fluoridated drinking water (CDC, 2016) in concentrations of ~700 µg/L (USDH, 2015). The addition of known quantities of F^- to drinking water makes it a suitable tracer for municipal water inputs to streams (USDH, 2015; Lockmiller et al., 2019). While inputs of F^- to natural waters in urban areas are generally from

municipal water inputs, F^- can also be introduced to streams (stream water concentrations ranging from 125-280 µg/L) in agricultural areas due to the application of F^--containing fertilizers (Stueber and Criss, 2005).

Wastewaters can be traced with B because the element is used as a bleaching agent in detergents, cleaners, and soaps used in households and businesses. Therefore, wastewaters have high B concentrations (Vengosh et al, 1994; USEPA, 2018). These B additions are not removed during use or during wastewater treatment (Vengosh et al., 1994; WHO, 1998; Hasenmueller and Criss, 2013). Other sources of B to the environment include glass manufacturing, flame retardants, cosmetics, antiseptics, pharmaceuticals, and agricultural fertilizers, but these are less common contributors. Previous work has shown that natural sources of B to waterbodies are generally uncommon, and that most B found in urban rivers is from anthropogenic sources, particularly wastewaters (Chetelat and Gallidardet, 2005; Guinoiseau et al., 2018).

High concentrations of OBs are ubiquitous in wastewater, relative to natural waters, due to their prevalence in laundry detergents and paper products as brightening agents (Tavares et al, 2008; Gholami et al., 2016). Untreated wastewaters have the highest OB concentrations, but ~55-98% of OBs are removed during the treatment process due to their adherence to the sludge (Poiger et al., 1998). This process results in lower OB concentrations in treated wastewater compared with untreated wastewater. Nevertheless, the high concentration of OBs in untreated wastewater makes them good tracers of unintentional releases of wastewater, such as those from leaking pipes and sewer overflows (Hartel et al., 2007; Cao et al. 2009; Billian et al., 2018; Lockmiller et al., 2019).

Previous work has shown that wastewater tracer concentrations are positively correlated to pipe proximity, impervious surface area (ISA), and urbanization (Vengosh et al., 1994, Wolf

et al., 2004, Lockmiller et al., 2019). Seasonally and during flood events, municipal water tracers have displayed both chemostatic and dilution trends. For example, Stueber and Criss (2005) noted that F^- concentrations remained constant seasonally and during floods. Concentrations of B diluted over the course of discharge events (Hasenmueller and Criss, 2013) and during wet seasons (Wyness et al., 2003) from the input of dilute rainwater in both urban and agricultural areas. In contrast, Lockmiller et al. (2019) found that B concentrations in an urban stream did not fluctuate seasonally or with discharge. Concentrations of OBs have been observed to behave chemostatically over seasons (Lockmiller et al., 2019), but dilution was observed during shorter term events like floods (Hayakawa et al., 2007). The variable responses in tracer behavior could be due to many factors including urbanization and ISA, age of infrastructure, proximity to municipal pipes, and antecedent moisture conditions in basins, but the exact mechanisms that control their behaviors are unclear. Understanding what controls variability in municipal tracers is critical for determining their utility in locating faulty municipal water infrastructure.

To our knowledge, only one study (Lockmiller et al., 2019) distinguished between drinking water and wastewater end-member inputs to streams. However, this study collected only a few samples from 18 watersheds across >1,000 km^2 in the Saint Louis, Missouri, United States, metropolitan area, and only sampled each stream twice over two years. The sampling method used in this study therefore lacks the spatial and temporal resolution necessary to understand fluctuations of municipal water inputs in headwater stream systems, where these municipal contributions likely impact aquatic life and people the most. Thus, this study seeks to use high resolution spatial and temporal sampling in an urban watershed (Deer Creek near Saint Louis, Missouri, United States) to identify how municipal drinking waters and wastewaters vary across a headwater catchment in space and time. Our efforts will establish the application of

these tracers at scales important to utilities and water managers. Understanding the impacts of municipal drinking waters and wastewaters on water resources is imperative to locate areas of contamination that could impact human and aquatic life and prevent waste of water resources.

CHAPTER 2: STUDY SITE

The focus of our study is the upper Deer Creek watershed, a small (19.31 km^2), urban catchment west of Saint Louis, Missouri, United States (Fig. 1A-B). The catchment is roughly aligned from the northwest to the southeast. Approximately 27.5% of the basin area is ISA, with developed areas generally decreasing from the headwaters to the mouth (Fig. 1C). Cultivated grasses are common in the catchment, but deciduous tree species are found in less developed areas of the watershed. Basin geology consists of Pennsylvanian shales in the northeast and Mississippian limestones in the southwest, with the two lithologies generally divided along the mainstem of Deer Creek (Harrison, 1997). Wastewater infrastructure occurs throughout the catchment, but is most concentrated along the main channel of Deer Creek (Fig. 1D). The outlet of the stream is located at the Litzsinger Road Ecology Center (LREC), which consists of ~0.14 km^2 of restored prairie and forest land. A United States Geological Survey (USGS) stage and discharge gauging station (station number = 07010055) is located ~300 m downstream of the LREC property (Fig. 1; green triangle); data from this station were used for our study.

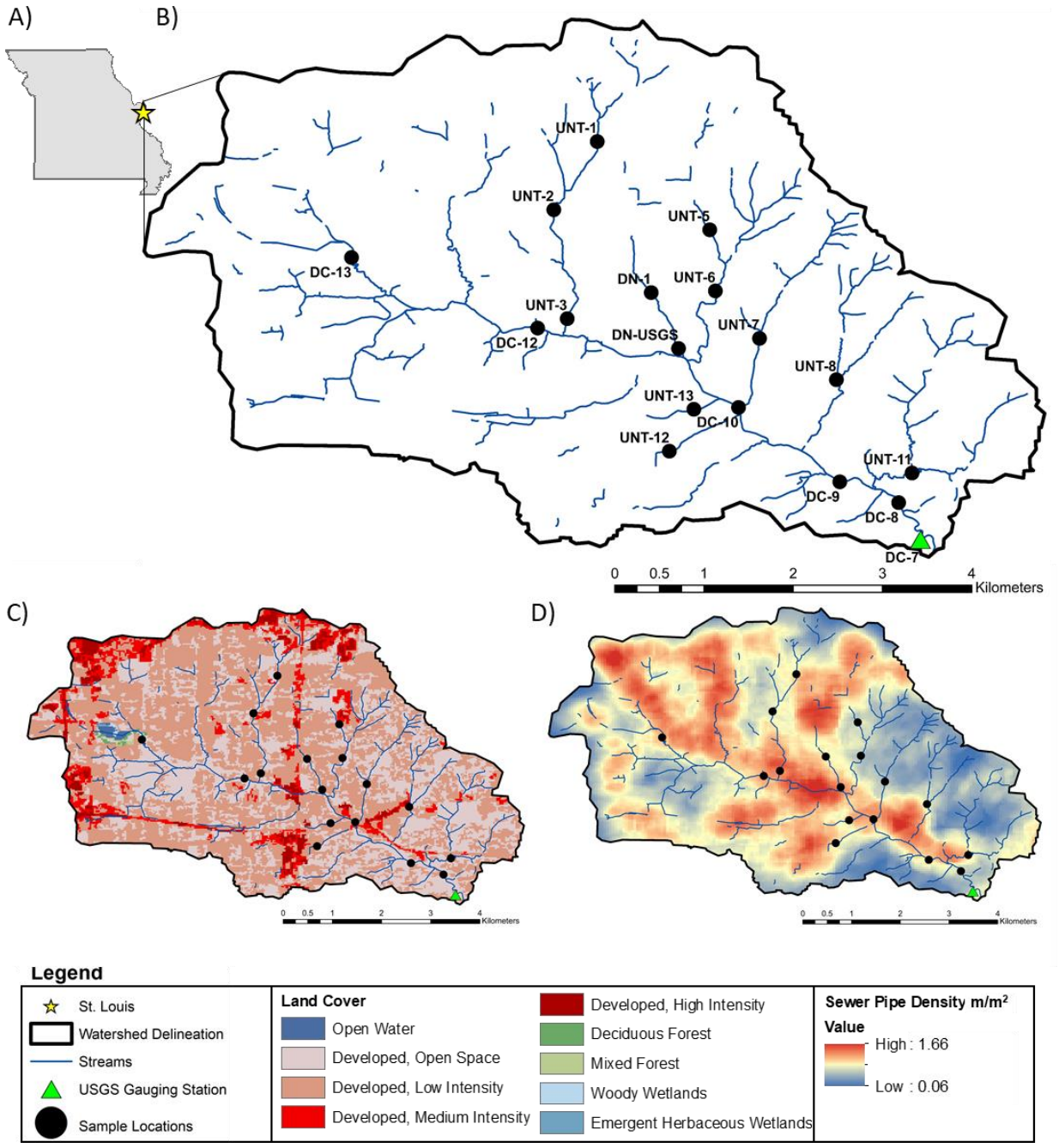

Figure 1. A) Map of Missouri denoting the location of the Deer Creek watershed in St. Louis with the B) study sampling locations, C) land use and land cover attributes (Homer et al., 2015), and D) sanitary and storm sewer pipe densities (MSD, unpublished).

CHAPTER 3: METHODS

3.1. Sampling Procedure

Within the upper Deer Creek watershed, we chose sites to characterize the municipal water inputs over the entire headwater catchment by including the mainstem and tributaries (Fig. 1). Sites were selected based on their spatial relationship to water infrastructure, but also for their accessibility and to avoid ephemeral reaches of the stream. Sampling was conducted bimonthly, spanning from November 2018 to November 2019 (i.e., seven sampling suites). We initially sampled eight sites, but increased this number to 18 by the end of the study (Table A1; Fig. 1). An effort was made to sample all sites during field campaigns, but accessibility periodically prevented sampling at certain sites. The site at the outlet of the catchment (Site DC-7 at LREC, near the USGS gauging station; Fig. 1) was sampled weekly to assess changes in municipal water inputs over shorter timeframes. The same site was sampled at higher frequency during one flood event to identify rapid changes in municipal water inputs during flow perturbations.

Bimonthly spatial and weekly temporal sampling (at the outlet; Site DC-7) consisted of in situ measurements of temperature, specific conductivity, Cl^-, dissolved O_2, and pH with a YSI ProPlus, turbidity with a Hach Turbidimeter, and OBs with a Turner Designs Aquafluor Handheld Fluorometer (Table 1, A2). In addition to in situ measurements, stream samples were collected to analyze for municipal water tracers and major element chemistry. The major element data were used to assess changes in groundwater inputs to Deer Creek, especially during winter months. Stream samples were field-filtered through 0.2-µm filters into two 50-mL polypropylene vials; one aliquot was for ion chromatographic (IC) analyses of F^- and Cl^-, while the other was acidified to 1% HNO_3 for analysis of B and major elements (Ca, Mg, Na, K, and Si) on an

inductively coupled plasma optical emission spectrometer (ICP-OES). All samples were kept frozen until analysis.

High frequency samples were collected during one flood event at the basin outlet (Site DC-7) in April 2019. Flood samples were collected with an ISCO 6712 autosampler. The autosampler collected ~1-L samples in low density polyethylene bottles at ~30-minute intervals during the rising limb of the flood and ~1-h intervals during the falling limb of the flood. Flood samples collected by the autosampler were returned to the lab where subsamples were analyzed for OB levels (within 24 h of sample collection). Separate aliquots were filtered through a 0.45-μm filter for F^- and Cl^- analysis (no additional treatment) and B and major element analysis (addition of HNO_3 to 1%). An in situ YSI EXO2 Multiparameter Sonde installed at Site DC-7 (the outlet) collected continuous (i.e., 5-minute interval) measurements of temperature, specific conductivity, Cl^-, dissolved O_2, pH, and turbidity.

To characterize the wastewater end-member, we obtained wastewater samples from the Metropolitan St. Louis Sewer District (MSD) from the WTP that services the Deer Creek basin (i.e., MSD's Lemay facility) for our September and November 2019 sampling days. We collected 24-h composites of both influent and effluent wastewater for each day we conducted spatial sampling. These samples were collected the next business day after spatial sampling occurred. Wastewater samples were processed immediately in the same way that the bimonthly spatial and weekly temporal samples were processed.

3.2. Lab Analyses

A Thermo Fisher Scientific Integrion Dionex IC was used to analyze F^- and Cl^- concentrations in our water samples. A PerkinElmer Optima 8300 ICP-OES was used to measure B and other major elements (Ca, Mg, Na, K, and Si). Instrument accuracy and precision for each

measured analyte was tested using check standards, blanks, and sample replicates, and was respectively within 6.1% and 0.4% for the IC and 5.0% and 3.5% for the ICP-OES. Due to equipment malfunctions and the COVID-19 global pandemic, we were unable to complete analyses of the drinking water tracer, F^-, so these data are not available. We also have an incomplete dataset for B and major elements.

3.3. Two-Component Mixing Model to Determine End-Member Inputs to a Headwater Stream

We used a two-component mixing model after Lakey and Krothe (1996) and Lee and Krothe (2001) to determine end-member inputs of natural water (*N*; i.e., unimpacted stream water collected from rural streams in the area) and wastewater (*W*; i.e., wastewater influent) end-members to the stream (*S*) samples:

$$Q_S C_S = Q_N C_N + Q_W C_W \quad (1)$$

$$C_S = \alpha_N C_N + \alpha_W C_W \quad (2)$$

$$1 = \alpha_N + \alpha_W \quad (3)$$

where Q is discharge and C is the concentration of the tracer of interest. Chemistries for the end-members were used to determine the relative contribution (α) of each end-member to each stream sample. The natural water and wastewater end-member chemistries were defined using OB data for regional rural streams and wastewater chemistries presented in Lockmiller et al. (2019) as well as OB data obtained from MSD's Lemay WTP during the time of sampling. We were unable to determine drinking water (*D*) contributions to the Deer Creek basin because we could not complete sample analyses of the drinking water tracer (F^-).

3.4. Spatial Analyses of Municipal Water Infrastructure Density and Tracer Concentrations

Sewer infrastructure densities in the upper Deer Creek watershed were derived from data obtained from MSD (MSD, unpublished). Raster data of sewage lines were processed in ArcMap

10.4.1 using the Line Density function. The output of this function resulted in a “heat” map of sewage infrastructure (Fig. 1D). We also calculated the density of sanitary and storm pipe infrastructure in the subcatchment draining to each sampling site in the basin (Table A1). Drinking water infrastructure data were unavailable for the project due to security concerns. Municipal water tracer concentrations, measured during our bimonthly spatial sampling events, were also converted to heat maps using the Inverse Distance Weighting (IDW) geoprocessing tool, set to power 5 and the extent expanded to include the entire watershed, in ArcMap 10.4.1.

CHAPTER 4: RESULTS

4.1. Spatial Trends in Municipal Water Tracers over Seasonal Timescales

We analyzed our bimonthly municipal water tracer (OB and B) and major element (Ca, Mg, Na, Cl^-, K, and Si) datasets for the Deer Creek watershed and MSD's Lemay WTP (Table 1) to assess spatial trends and the impact of seasonality on water sourcing within the catchment. Data for OB and major ions are available for the entire duration of the spatial study. However, B data are only available from November 2018 to June 2019 due to disruptions in lab activities from the COVID-19 global pandemic.

Over the 1-year duration of our study, OB concentrations ranged from 11.88 to 38.17 RFU, with an average of 20.56 ± 4.67 RFU. The lowest OB concentration occurred in March 2019 at a tributary location close to the northern headwaters (Site UNT-2; Fig. 2). The March 2019 sampling event followed 2.72 cm of precipitation during the three days prior to sampling (Fig. 3). The highest OB concentration occurred in September 2019 at a northern tributary near the outlet (Site UNT-7; Fig. 2). In the three days prior to the September 2019 sampling event, there was no precipitation (Fig. 3). Seasonally, OB concentrations were generally lowest in the western and northern headwater tributaries and highest in the northeastern tributaries near the outlet. Lower, catchment-wide concentrations occurred from January 2019 to July 2019, while higher concentrations across the watershed were observed from September 2019 to November 2019 (Table A3, Fig. 2).

Table 1. Average (± standard deviation) analyte concentrations for each subbasin sampling location and influent and effluent wastewater samples.

Site	Date	OB (RFU)	B (µg/L)	Cl (mg/L)	Ca (mg/L)	Mg (mg/L)	Na (mg/L)	K (mg/L)	Si (mg/L)
DC-7		18.55 ± 1.04	57.19 ± 4.11	385.12 ± 134.54	91.67 ± 12.04	26.04 ± 7.61	223.28 ± 86.05	32.17 ± 26.99	3.30 ± 0.46
DC-8		20.15 ± 1.09	59.53 ± 5.76	470.82 ± 146.84	107.01 ± 16.62	35.90 ± 10.77	311.59 ± 106.74	65.91 ± 39.69	3.62 ± 0.36
DC-9		19.99 ± 1.29	61.11 ± 6.83	412.14 ± 153.76	97.84 ± 16.34	30.16 ± 10.52	236.87 ± 96.57	41.59 ± 36.51	3.59 ± 0.44
DC-10		20.40 ± 0.89	57.28 ± 3.34	359.84 ± 157.42	88.98 ± 21.06	29.13 ± 12.63	226.51 ± 111.25	48.48 ± 43.50	3.81 ± 0.58
DC-12		18.47 ± 0.93	43.22 ± 2.97	314.64 ± 110.31	89.18 ± 22.48	29.70 ± 13.27	217.28 ± 99.52	43.42 ± 38.58	3.99 ± 0.74
DC-13		18.57 ± 0.93	35.61 ± 2.11	214.49 ± 64.08	58.18 ± 11.86	20.96 ± 6.98	128.01 ± 42.83	16.86 ± 12.25	2.98 ± 0.58
DN-1		23.61 ± 0.48	62.95 ± 8.48	350.82 ± 77.35	107.30 ± 6.81	33.91 ± 6.08	204.77 ± 48.51	29.69 ± 23.97	5.67 ± 0.44
DN-USGS		23.08 ± 0.44	61.96 ± 13.71	288.29 ± 68.81	102.14 ± 4.66	30.18 ± 5.85	177.67 ± 52.10	29.46 ± 23.91	4.00 ± 0.65
UNT-1		18.13 ± 0.67	64.15 ± 21.64	642.72 ± 67.77	120.78 ± 8.16	46.62 ± 7.49	387.59 ± 59.11	39.71 ± 32.95	5.47 ± 0.58
UNT-2		18.53 ± 1.65	65.83 ± 5.51	461.76 ± 132.95	102.63 ± 17.45	38.41 ± 10.23	286.92 ± 101.49	47.00 ± 41.27	4.66 ± 0.70
UNT-3		19.34 ± 1.20	54.54 ± 14.00	510.84 ± 232.23	114.25 ± 27.36	39.83 ± 16.26	339.83 ± 186.66	77.31 ± 71.75	3.86 ± 0.65
UNT-5		18.72 ± 1.29	55.22 ± 15.49	369.88 ± 45.16	98.88 ± 6.43	35.75 ± 4.93	196.46 ± 37.58	21.23 ± 16.28	6.02 ± 0.53
UNT-6		20.91 ± 1.41	68.34 ± 5.27	279.04 ± 52.39	99.11 ± 5.55	32.30 ± 5.51	166.91 ± 32.58	23.08 ± 16.93	5.25 ± 0.68
UNT-7		30.48 ± 2.86	66.33 ± 18.23	85.73 ± 12.36	82.80 ± 5.63	23.83 ± 2.97	63.36 ± 5.42	11.03 ± 4.84	5.42 ± 0.83
UNT-8		28.58 ± 2.17	64.13 ± 15.00	123.54 ± 38.16	72.00 ± 3.23	24.44 ± 5.61	81.19 ± 21.16	17.52 ± 11.74	4.28 ± 0.64
UNT-11		26.67 ± 2.40	45.52 ± 14.16	114.73 ± 36.20	62.52 ± 9.22	16.95 ± 5.75	65.29 ± 15.59	12.91 ± 8.01	4.17 ± 1.32
UNT-12		22.46 ± 2.34	-	-	144.52 ± 48.99	51.19 ± 26.88	417.13 ± 300.23	120.12 ± 113.29	5.62 ± 1.98
UNT-13		17.11 ± 1.13	-	-	90.12 ± 30.34	33.54 ± 17.20	294.82 ± 207.37	84.10 ± 79.21	3.94 ± 1.42
Lemay Influent	9/15/2019	65.88	-	93.54	73.08	21.68	84.38	11.14	1.99
Lemay Effluent	9/15/2019	23.79	-	95.82	42.68	12.30	47.55	24.52	3.30
Lemay Influent	11/19/2019	66.61	-	-	51.92	32.32	98.23	39.51	5.85
Lemay Effluent	11/19/2019	28.45	-	-	69.09	-	-	-	-

The B concentrations (available from November 2018 to June 2019) ranged from 31.36 to 106.87 μg/L, with an average of 56.74 ± 16.62 μg/L. The lowest concentration of B occurred in March 2019 at a northern tributary location near the outlet (Site UNT-11). Total precipitation in the three days prior to the sampling event was the highest value observed during the study (2.72 cm; Fig. 3). The highest B concentrations occurred in November 2018 at a headwater tributary location (Site UNT-1; Fig. 2), which had 0.20 cm of precipitation in the three days prior to the sampling event (Fig. 3). Northwestern headwater sites and locations near the outlet consistently had lower B concentrations than the other sampling sites (Fig. 2). Our limited dataset shows that the average B concentration was lowest in the wettest sampling month (i.e., March 2019; Table A3).

Specific conductivity and most of the major ions (Cl^-, Ca, Mg, Na, and K) were significantly correlated with each other ($p < 0.05$), so we observed similar trends in these elements across space and time for the Deer Creek watershed (Tables 1, A3, A4; Figs. 2, A1). Here, we focus on the trends in Cl^- (Fig. 2), as they are representative of the other major element (e.g., Ca and Na; Tables 1, A4; Fig. A1) spatial patterns with time. Seasonal trends in Cl^- helped us identify groundwater inputs during winter months. Concentrations for Cl^- ranged from 49.91 to 1421.98 mg/L over the study period, with an average of 361.17 ± 31.10 mg/L. The lowest concentration of Cl^- occurred in June 2019 at a northern tributary location near the outlet (Site UNT-11). This sampling date had the second highest precipitation total for the three days prior to sampling (2.13 cm; Fig. 3). The highest Cl^- concentrations occurred in November 2019 at a northern, midbasin tributary (Site UNT-3; Fig. 2); for the three days prior to this sampling date, there was 0.03 cm of precipitation. We observed the highest average Cl^- concentrations and ranges across the Deer Creek catchment during the winter months (Table A3; Fig. 2), when

deicing salts were applied to roadways in the basin. Like the OB and B datasets, Cl^- concentrations were lowest in the northwestern headwaters. However, three northeastern tributary locations near the outlet also consistently had low Cl^- concentrations, despite higher OB and B values at these sites. We found that Si was significantly and positively correlated ($p < 0.05$) with Cl^-, but not the other major elements (Table A4). The Si values were also significantly ($p < 0.05$) and positively correlated with both the wastewater tracers (OB and B; Table A4).

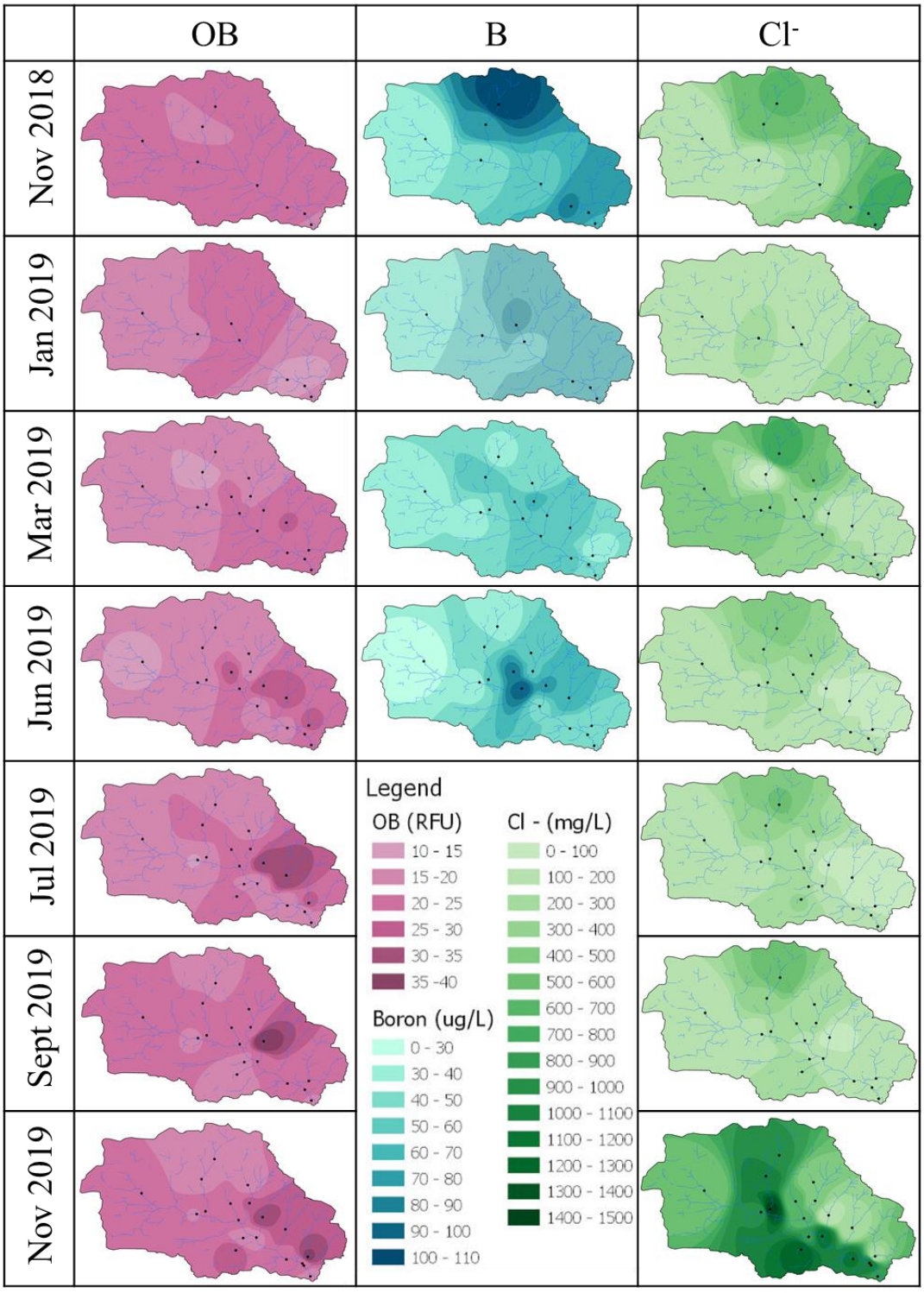

Figure 2. Spatial interpolations of OB, B, and Cl^- data for each sampling event over the 1-year study period. Averages, ranges, minima, and maxima for each spatial sampling event are available in Table A3.

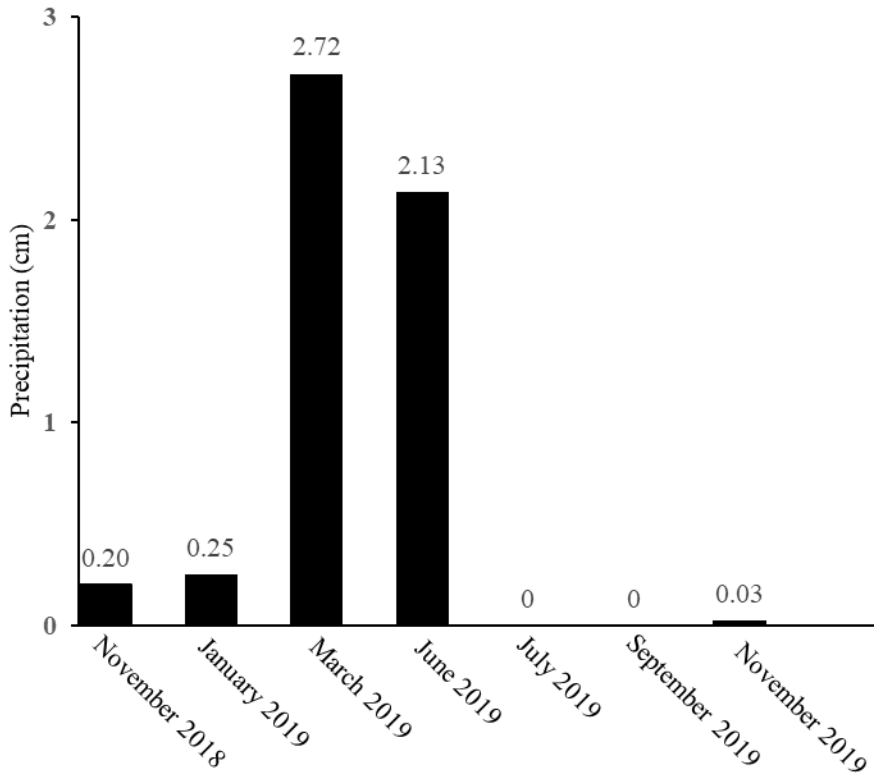

Figure 3. Precipitation totals for the three days prior to each sampling event. Data were collected at St. Louis Lambert International Airport, St. Louis, MO (NOAA, 2020).

The relationship between our wastewater tracers, OB and B, in our spatial samples was found to be positive, but insignificant (p = 0.052; Fig. 4), possibly because of our limited B dataset. We compared our OB and B tracer data for the spatial sampling suites at Deer Creek with natural water and wastewater end-member compositions (Fig. 5). Since we were unable to obtain a full suite of B data for our samples (including our wastewater), we compared our available OB and B concentrations in the Deer Creek catchment to natural water, wastewater, and drinking water tracer values for the St. Louis region presented by Lockmiller et al. (2019). We found that our samples fell within a mixing triangle (Fig. 5), and had intermediate values compared with average values for rural streams (29 μg/L and 3.7 RFU), drinking water (82 μg/L and 5.5 RFU), and wastewater (212 μg/L and 105 RFU; Lockmiller et al., 2019).

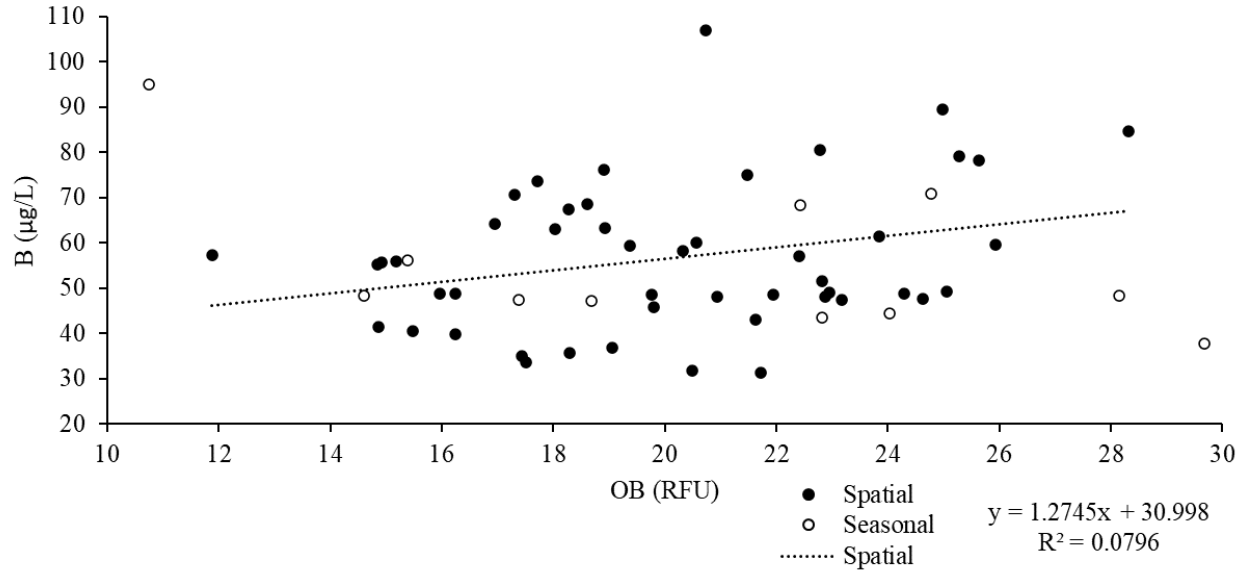

Figure 4. Spatial (bimonthly samples from November 2018 to June 2019; black circles) and seasonal (weekly samples from November 2018 to February 2019) OB and B values for samples collected in the Deer Creek watershed.

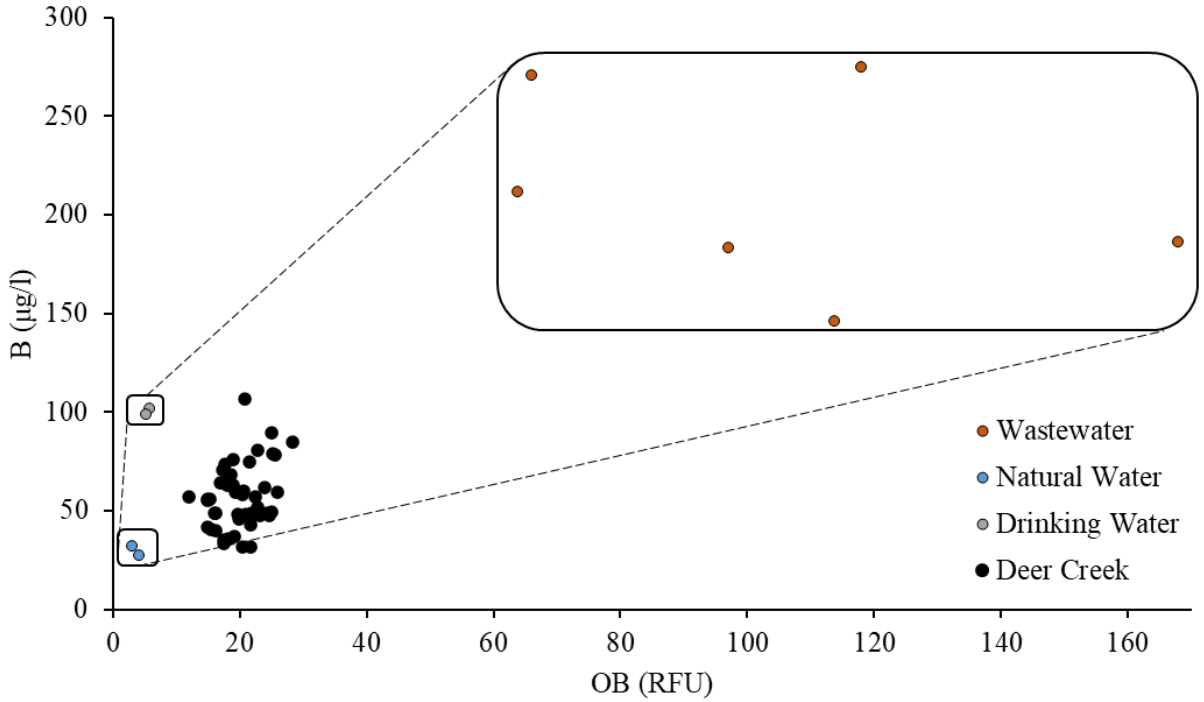

Figure 5. Concentrations of OB and B for our samples collected at Deer Creek compared with concentrations previously obtained by Lockmiller et al. (2019) for end-member compositions (i.e., natural water, wastewater, and drinking water) in the St. Louis region.

With the OB data collected at the spatial sites (our only complete municipal water tracer dataset), we used a two-component mixing model to understand the percent contribution of wastewater to each of the Deer Creek sites across space and time. On average, Deer Creek was comprised of 27.79 ± 7.35% wastewater, ranging from 13.13 to 55.14% of the total stream volume during the sampling period. We compared our OB concentrations and calculated wastewater inputs to the densities of sanitary, storm, and all (the combination of sanitary and storm) wastewater piping for the subcatchments draining to each sampling site (Table 2). We found that both OB concentrations and wastewater inputs had a significant, negative relationship with sanitary pipe density ($p < 0.05$), but no relationship with storm pipe density ($p > 0.05$; Table 2; Fig. 6). Stream B levels had an insignificant ($p > 0.05$) relationship with both types of infrastructure (Table 2). None of our major element concentrations had significant correlations with any of the pipe density types (Table A4). Lastly, we saw that our wastewater tracers showed no correlation with ISA in the watershed (Table 2).

Table 2. Pearson correlations for spatial data for wastewater tracers and wastewater infrastructure (bold text denotes a significant *p* value for the correlation).

	OB (RFU)	B (µg/L)	Cl^- (mg/L)	Wastewater (%)	Natural Water (%)	Sanitary Pipe Density (m/km^2)	Storm Pipe Density (m/km^2)	All Pipe Density (m/km^2)	ISA (%)
OB (RFU)	1								
B (µg/L)	0.28	1							
Cl^- (mg/L)	-0.14	0.16	1						
Wastewater (%)	0.98	0.25	-0.15	1					
Natural Water (%)	-0.98	-0.25	0.15	-1	1				
Sanitary Pipe Density (m/km^2)	**-0.24**	-0.08	0.03	**-0.27**	0.27	1			
Storm Pipe Density (m/km^2)	-0.22	0.06	0.12	-0.22	0.22	0.10	1		
All Pipe Density (m/km^2)	**-0.30**	-0.05	0.06	**-0.32**	0.32	0.89	0.53	1	
ISA (%)	0.19	-0.05	-0.07	-0.59	0.59	0.25	0.10	0.26	1

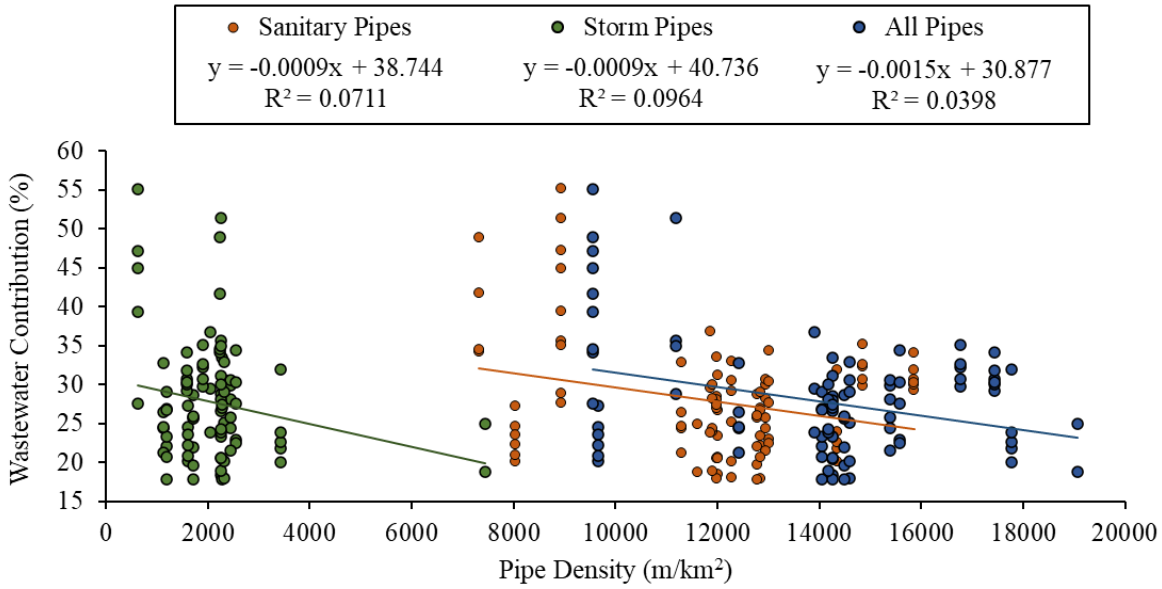

Figure 6. Percent wastewater contribution (calculated from our OB data) plotted against sanitary (orange), storm (green), and all (blue) infrastructure densities.

4.2. High Resolution Temporal Trends in Municipal Water Tracers

4.2.1. Seasonal Variations

We used our weekly grab sample data, collected at the outlet site (Site DC-7), to understand changes in municipal water tracer concentrations at higher temporal resolution. Over the year-long study, OB (n = 81) and B (n = 14) concentrations varied between 9.92 and 32.61 RFU and 37.72 and 95.05 µg/L, respectively. Due to the limited amount of B data (Fig. 7), we are unable to assess seasonal variance in B at our outlet site. Major element data for temporal samples at the outlet site are unavailable.

We found that there was no significant (p > 0.05) relationship for OB concentrations as a function of time for the entire study (November 2018 to November 2019). However, to understand the change in wastewater tracers over strictly one year, the first month of sampling data were excluded from calculations. Excluding these data ensured that the trend of the previous year would not confound the results. In this case, concentrations of OB significantly increased (p

= 0.00) from December 2018 to November 2019 (Fig. 7). We found no significant change in OB or B concentrations as a function of discharge (p = 0.90 and p = 0.95, respectively; Fig. 8).

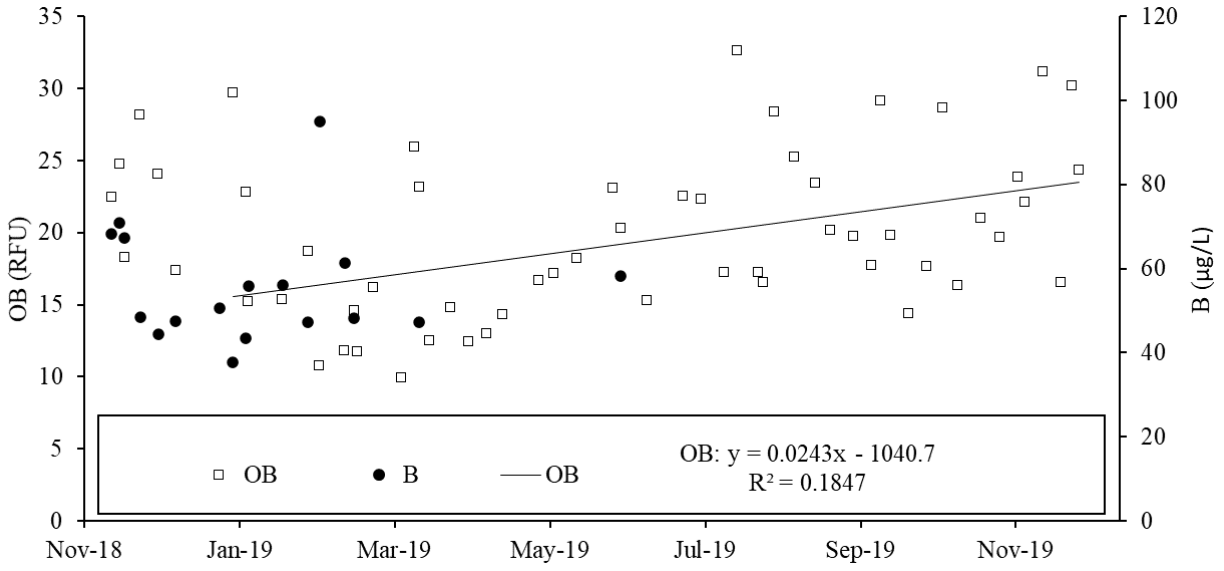

Figure 7. Concentrations of OB and B over time at the outlet site (Site DC-7) for November 2018 to November 2019. The OB trendline is interpolated through the December 2018 to November 2019 data to show changes in OB values over strictly one year. We found a significant (p < 0.05), positive relationship between OB and time.

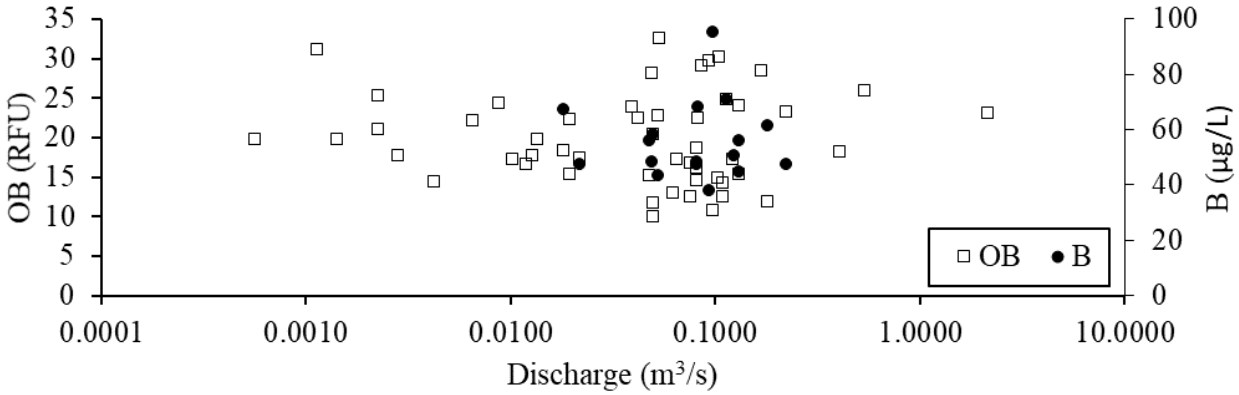

Figure 8. Concentrations of OB and B with discharge at the outlet site (Site DC-7). We found no correlation (p > 0.05) for OB or B with discharge.

When we used OB concentrations to calculate the percent wastewater inputs to the stream outlet site, we found that wastewater contributed between 9.9 and 46.3% of the total stream volume, averaging at 26.02 ± 9.0%. We saw a significant relationship between wastewater contributions and time (p = 0.04; Fig. 9) for December 2018 to November 2019. The increase in wastewater contributions over time was expected, because the data were derived from OB concentrations, which also increased over the one-year period. There was no significant relationship between wastewater inputs and discharge (p = 0.49; data not shown).

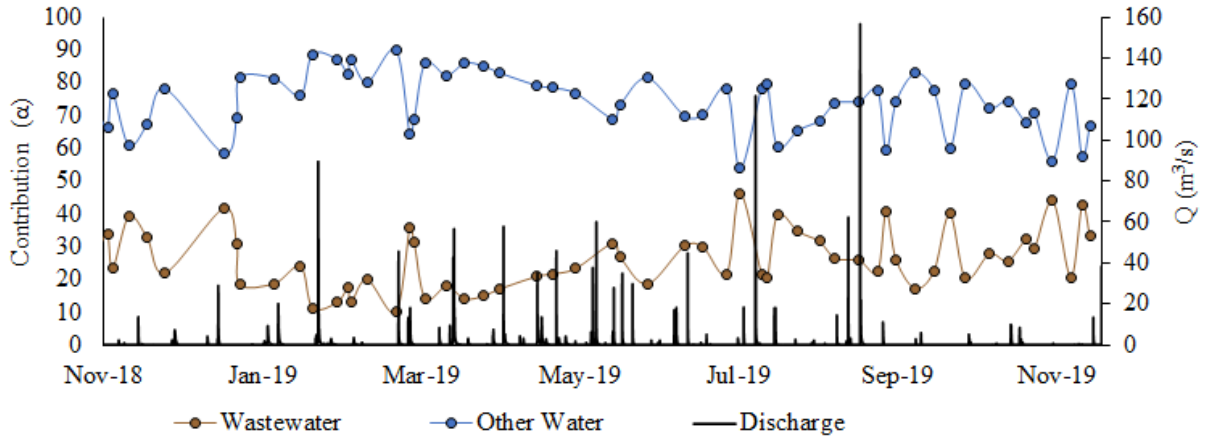

Figure 9. Percent contribution of wastewater and other water (the combination of drinking water and natural water; calculated with OB concentrations) plotted with discharge over time.

4.2.2. Flood Event Variations

While we did not observe significant changes in OB concentrations as a function of discharge on seasonal timescales (Fig. 8), we did observe OB concentration changes associated with discharge perturbations on shorter timescales (i.e., flood responses; Fig. 10). We characterized one flood event at the outlet site (Site DC-7) that began on 11 April 2019. Prior to the event, stream baseflow was ~0.05 m^3/s, but discharge rapidly peaked at 0.44 m^3/s. Following peak flow, stream flow gradually decreased to baseflow levels over approximately 1 day. The

OB concentrations varied between 15.54 and 25.15 RFU during the flood. Initially, OB values did not vary more than ~3 RFU as discharge rapidly increased to its highest values. However, OB concentrations increased after peak discharge and peaked in concentration during the recessional limb of the hydrograph (lagging the discharge peak by 5 h). Concentrations of OBs then slowly decreased to baseflow levels only after discharge decreased to values of about 0.1 m^3/s (Fig. 10). Other tracer and major element data are unavailable for this flooding event.

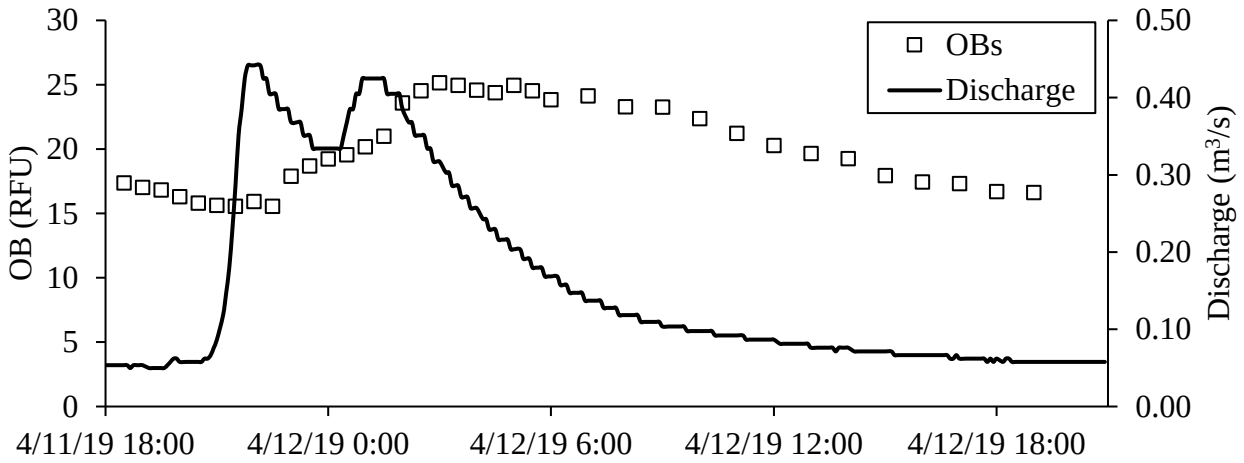

Figure 10. The flood hydrograph and OB chemograph for the 11 April 2019 flood at the Deer Creek outlet site (Site DC-7).

CHAPTER 5: DISCUSSION

5.1. Spatial Variations in Municipal Water Inputs

We found that wastewater tracers (OB and B) varied with space and time across our headwater catchment. The higher resolution spatial and temporal sampling regime for this study, compared to previous research, showed that patterns of municipal water tracers were not always predicted by infrastructure and land use attributes. Previous studies have observed a positive correlation between wastewater tracers and wastewater infrastructure density (due to leaking pipes; Wolf et al., 2006; Wolf et al., 2004) as well as ISA (Lockmiller et al., 2019). We saw that OB and B had a positive correlation, which was expected since they are both wastewater tracers. Nevertheless, the correlation was not significant, likely because of the limited B dataset. We unexpectedly found that OB concentrations negatively correlated with the amount of infrastructure density and have no significant relationship with ISA. Our data suggest that high densities of wastewater infrastructure and urban development do not necessarily equate to locally high inputs of wastewater to streams at finer scales. Thus, wastewater inputs across Deer Creek at the watershed scale do not align with findings from earlier studies conducted at the regional scale.

While we do not have complete tracer (B and F^-) and major element datasets, which makes discerning municipal water inputs more difficult, we suspect that localized groundwater flow may be driving the patterns we observed in the wastewater tracers. We used our Cl^- data during the winter months (e.g., November 2019) to indicate where there might be higher inputs of groundwater to the stream. During road deicing periods, the groundwater would be relatively dilute compared to surface water as road salts are flushed from ISA via surface runoff. Thus, groundwater inputs to the stream likely occurred were stream Cl^- concentrations were relatively

low. During the November 2019 sampling date, Cl^- was elevated across the catchment following a winter road salting event (Fig. 2). However, three northeastern tributary locations near the outlet (i.e., Sites UNT-7, UNT-8, and UNT-11) had much lower Cl^- values (Fig. 2), suggesting that, at these locations, dilute groundwater may have been entering the stream. Higher inputs of groundwater along this section of the watershed is consistent with basin geology at this location, where shales transition to carbonates. These same sites also had relatively higher OB concentrations, even though pipe and ISA densities for these locations were low. Moreover, we observed a strong correlation between Si concentrations and wastewater tracer values. Groundwater often features elevated levels of Si compared to surface water due to subsurface bedrock weathering. Thus, higher Si concentrations in the stream likely indicate higher groundwater inputs that feature elevated wastewater tracer values. Taken together, our chemical data suggest that groundwater contaminated with wastewater was being transported into the stream through the hyporheic zone at these locations (Passarello et al., 2012; Keefe et al., 2019).

We also observed changes in tracer and major element chemistries across the watershed that were likely due to recent rainfall events rather than changes in municipal wastewater inputs (i.e., changes in wastewater leakage rates were unlikely to cause these variations because wastewater volumes are relatively constant over time). During the months of January 2019 to June 2019, OB had relatively low concentrations, likely due to wetter conditions across the basin in the days prior to sampling events (Table A3; Figs. 2, 3). During the months of July 2019 to November 2019, OB had higher averages and larger concentration ranges across the catchment (Table A3; Fig. 2), suggesting that drier conditions (Fig. 3) prior to sampling led to more variability in tracer concentrations. Major element concentrations were also driven, in part, by antecedent moisture conditions. However, high concentrations of the major elements in the

winter (Figs. 2, A1) were due to the application of road salt, which subsequently entered the stream after precipitation events. Our chemical results show that wastewater tracers, like OB and B, are probably influenced by recent precipitation events, so fluctuations in recent antecedent moisture conditions need to be considered when utilizing these tracers.

We observed that at the catchment scale, wastewater tracers did not necessarily correlate with wastewater infrastructure density as seen in other large scale studies. Rather, the distribution of wastewater inputs in the Deer Creek watershed may be driven by local groundwater flow patterns and recent precipitation events. This result could confound attempts to locate faulty infrastructure on finer scales. However, at regional scales, localized groundwater flow patterns are less important, which likely explains why previous studies with larger spatial extents have observed the positive correlation between wastewater tracers and infrastructure. Thus, wastewater tracers may be useful at regional scales, but may become less effective at the catchment scale, particularly in catchments with heterogenous lithology like Deer Creek.

5.2. Temporal Variations in Municipal Water Inputs at the Outlet Site

At our outlet site, OB concentrations increased significantly over time in weekly samples from December 2018 to November 2019. Unlike our study, a study by Lockmiller et al. (2019) did not see any significant changes in OB concentrations over time at the Deer Creek monitoring site, which could be due to their study's shorter monitoring period (i.e., 6 months). The seasonal increase in OB concentrations observed in our dataset is somewhat perplexing, but may be related to the decreased precipitation amounts throughout the year (Fig. 3). Lower precipitation could cause the accumulation of wastewater in groundwater without dilution. Our B concentrations did not change with time, but the B dataset was incomplete.

Weekly concentrations of OB and B at the outlet site were not significantly related to discharge, instead showing a chemostatic response (Fig. 8). The chemostatic tracer response is inconsistent with previous studies by Hayakawa et al. (2007) and Hasenmueller et al. (2013), which both saw tracer dilution as discharge increased. However, our findings were consistent with the Lockmiller et al. (2019) study conducted at the Deer Creek outlet site. The non-significant trend in OB and B concentrations with discharge may be due to the observed lag in wastewater tracer response following discharge perturbations (Fig. 10). This difference in timing may be driving the seemingly "chemostatic" response of the municipal water tracers observed in the weekly samples. Moreover, our weekly samples were generally collected under low flow conditions, which may also explain the non-significant relationship between the tracers and discharge.

The decoupling of the discharge and OB responses may be due to either the lag in time it takes for precipitation to activate sewer overflows during the flood event or slower, contaminated groundwater reaching the stream. A CSO upstream of our outlet sampling site can activate during flooding. However, the CSO was unlikely to have activated during the April 2019 flood considering the relatively low discharge peak for this event. Instead, the lag in OB response during floods may be due to inputs of groundwater contaminated with wastewater. Groundwater inputs during floods at this site are known to lag peak discharge (Deeba and Hasenmueller, 2018), possibly explaining these timing differences.

Regardless of the source of high OB concentrations during the flood, this increase in concentration as the flood progressed conflicts with findings from Hasenmueller and Criss (2013), who showed dilution of another wastewater tracer (B) in stream samples during flood events. The municipal water tracer dilution observed by Hasenmueller and Criss (2013) may

have been caused by several factors, such as the amount of urbanization in the studied watershed, age of municipal water infrastructure, and, most notably, the discharge volumes in the studied floods. The discharge volume for our recorded flood was relatively small (0.44 m^3/s), while the floods in Hasenmueller and Criss (2013) were much larger (up to 14 m^3/s). Thus, tracer dilution may become increasingly important with higher discharge volumes.

CHAPTER 6: CONCLUSION

Previous studies that have sampled at large spatial scales and lower frequencies found that municipal water inputs positively correlate with infrastructure density and land use characteristics, like ISA. However, these large spatial extents may be less useful to utilities and water managers who need to identify the impacts of municipal water releases at the watershed scale. To our knowledge, our study is the first to assess municipal water inputs at high spatial and temporal resolution within a small headwater catchment. Using municipal water tracers, such as OB and B, we were able to identify variability in the wastewater signature at small scales in space and time. Our results show that infrastructure and land use do not always predict spatial and temporal trends of municipal water tracers at the catchment scale.

Instead, the spatial and temporal patterns in municipal water tracers for smaller watersheds like Deer Creek are likely influenced by groundwater flow patterns across the basin as well as by antecedent moisture conditions. Groundwater inputs to streams, driven by catchment lithology, can move wastewater contaminants from areas of high pipe density to areas of low pipe density, leading to high concentrations of wastewater tracers that would not be predicted by infrastructure location data. Indeed, during our study, we found that sites with high wastewater contributions coincided with areas that were more influenced by groundwater inputs than by infrastructure and development densities. Total wastewater volumes conveyed by pipes in the catchment are unlikely to be changing substantially over time. Instead, our data suggest that wetter basin conditions dilute municipal water signatures, while drier conditions allow for the accumulation and increased variability in tracer concentrations.

Previous studies at regional scales have successfully shown that municipal water tracers are positively correlated with water infrastructure and development density. However, our data

show that high concentrations of these tracers are not necessarily driven by infrastructure and development densities at the catchment scale. Therefore, our efforts have established the importance of utilities and water managers knowing localized groundwater flow and antecedent moisture conditions when using municipal water tracers to detect faulty infrastructure at catchment scales.

APPENDIX

Table A1. Location, drainage area, ISA, and wastewater infrastructure characteristics for each subbasin sampling location.

Site	Latitude (°)	Longitude (°)	Drainage Area (km^2)	ISA (%)	Sanitary Pipe Length (m)	Sanitary Pipe Density (m/km^2)	Storm Pipe Length (m)	Storm Pipe Density (m/km^2)	All Pipe Length (m)	All Pipe Density (m/km^2)
DC-7	38.62239	-90.37542	19.31	27.50	231985.11	12012.44	43483.38	2251.62	275468.49	14264.05
DC-8	38.62735	-90.37886	19.15	27.60	229528.42	11985.10	43455.95	2269.10	272984.37	14254.21
DC-9	38.62956	-90.3848	17.38	28.40	213438.03	12280.05	40173.86	2311.38	253611.89	14591.44
DC-10	38.63741	-90.39577	13.70	29.60	177371.96	12951.13	33484.41	2444.92	210856.37	15396.05
DC-12	38.64506	-90.41523	6.73	29.60	85923.12	12772.80	11489.44	1707.95	97412.56	14480.74
DC-13	38.65235	-90.43409	2.35	34.90	30206.90	12855.99	2788.62	1186.83	32995.51	14042.82
DN-1	38.64847	-90.40351	0.64	30.80	9566.15	14860.36	1220.42	1895.84	10786.57	16756.20
DN-USGS	38.64299	-90.40115	0.77	29.80	12249.61	15857.44	1222.86	1583.02	13472.46	17440.46
UNT-1	38.66388	-90.40931	0.76	40.40	6087.16	8047.65	1221.94	1615.49	7309.10	9663.14
UNT-2	38.65611	-90.4137	1.54	33.00	17453.76	11297.18	1738.27	1125.12	19192.04	12422.30
UNT-3	38.6459	-90.41242	2.04	31.20	24341.33	11909.48	4631.74	2266.17	28973.07	14175.65
UNT-5	38.65497	-90.39815	0.76	32.50	10851.18	14346.02	2587.45	3420.79	13438.63	17766.81
UNT-6	38.64865	-90.39735	1.61	27.90	20936.10	13009.12	4115.41	2557.20	25051.51	15566.33
UNT-7	38.64387	-90.39302	0.63	20.30	5610.15	8938.44	388.62	619.17	5998.77	9557.62
UNT-8	38.63974	-90.38512	0.69	18.10	5064.56	7318.55	1550.52	2240.58	6615.07	9559.13
UNT-11	38.63038	-90.37761	1.50	20.50	13373.71	8935.55	3367.13	2249.72	16740.84	11185.27
UNT-12	38.63258	-90.40199	0.55	33.30	6487.97	11857.20	1118.01	2043.23	7605.98	13900.44
UNT-13	38.63675	-90.39963	0.53	36.10	6172.50	11622.50	3952.65	7442.63	10125.15	19065.13

Table A2. Average (± standard deviation) field-collected analyte concentrations for each subbasin sampling location and influent and effluent wastewater samples.

Site	Date	Temp (°)	DO (mg/L)	DO (%)	SpC (mg/L)	pH	Turbidity (NTU)
DC-7		15.10 ± 4.13	124.79 ± 46.83	7.90 ± 1.17	1,759.71 ± 465.63	7.67 ± 0.06	4.56 ± 1.14
DC-8		12.21 ± 3.25	87.28 ± 5.87	9.61 ± 1.04	2,071.50 ± 508.91	7.96 ± 0.05	3.57 ± 0.84
DC-9		13.31 ± 3.47	100.34 ± 7.15	10.78 ± 1.16	1,773.57 ± 461.19	8.07 ± 0.06	3.63 ± 0.99
DC-10		14.83 ± 3.77	90.73 ± 3.63	9.42 ± 1.03	1,669.33 ± 539.09	8.04 ± 0.03	4.04 ± 0.84
DC-12		14.01 ± 3.58	98.14 ± 4.19	10.42 ± 1.03	1,518.14 ± 393.77	7.88 ± 0.11	4.09 ± 0.53
DC-13		14.74 ± 3.84	87.11 ± 8.43	9.25 ± 1.45	1,097.76 ± 255.52	8.06 ± 0.11	8.75 ± 2.44
DN-1		14.18 ± 3.63	86.20 ± 11.52	8.85 ± 1.40	2,031.33 ± 452.74	8.22 ± 0.24	2.77 ± 0.56
DN-USGS		14.20 ± 3.65	82.50 ± 3.31	8.61 ± 0.81	1,568.50 ± 238.87	8.01 ± 0.07	3.22 ± 1.19
UNT-1		15.02 ± 4.17	100.10 ± 6.66	9.51 ± 0.74	2,722.83 ± 229.96	8.13 ± 0.08	1.88 ± 0.25
UNT-2		14.63 ± 9.13	82.25 ± 5.83	8.48 ± 0.88	2,041.02 ± 474.47	8.19 ± 0.11	1.95 ± 0.40
UNT-3		17.06 ± 4.17	100.62 ± 4.13	9.76 ± 0.80	2,255.00 ± 757.06	7.94 ± 0.06	3.27 ± 0.93
UNT-5		16.28 ± 4.00	89.52 ± 3.97	8.91 ± 0.95	1,845.20 ± 158.37	8.10 ± 0.17	2.15 ± 0.49
UNT-6		15.56 ± 4.11	83.76 ± 3.02	8.56 ± 1.00	1,135.28 ± 308.88	7.98 ± 0.10	2.26 ± 0.85
UNT-7		15.14 ± 4.13	43.54 ± 10.19	4.65 ± 1.44	755.46 ± 193.84	7.86 ± 0.28	7.10 ± 1.69
UNT-8		13.93 ± 4.19	70.53 ± 12.07	8.70 ± 0.90	1,012.50 ± 142.97	7.92 ± 0.04	4.49 ± 1.42
UNT-11		15.62 ± 3.75	59.78 ± 13.37	5.85 ± 1.42	851.72 ± 152.13	7.49 ± 0.10	18.69 ± 4.42
UNT-12		17.27 ± 5.09	101.50 ± 12.15	10.35 ± 0.69	1,189.43 ± 572.05	8.43 ± 0.17	1.02 ± 0.09
UNT-13		17.80 ± 4.26	84.30 ± 1.46	8.00 ± 0.82	2,069.00 ± 764.08	8.09 ± 0.13	1.56 ± 0.28
Lemay Influent	9/15/2019	8.3	10.23	88.9	2594	2.46	102
Lemay Effluent	9/15/2019	7.8	11.25	96.8	1858	2.64	18
Lemay Influent	11/19/2019	10.1	8.62	78.8	1493	2.98	8.04
Lemay Effluent	11/19/2019	10	4.76	43.6	3084	2.38	76.3

Table A3. Averages, ranges, minima, and maxima for each spatial sampling event.

OB (RFU)				
Date	Average (± Standard Deviation)	Range	Minimum	Maximum
11/21/18	20.84 ± 1.59	4.51	18.28	22.79
01/08/19	18.30 ± 3.65	8.99	14.85	23.84
03/15/19	20.27 ± 3.69	13.18	11.88	25.06
06/01/19	20.44 ± 4.23	13.46	14.86	28.32
07/26/19	20.95 ± 5.60	19.44	14.80	34.24
09/13/19	22.01 ± 4.66	21.50	16.67	38.17
11/18/19	22.54 ± 5.27	20.38	15.42	35.80
B (μg/L)				
Date	Average (± Standard Deviation)	Range	Minimum	Maximum
11/21/18	67.22 ± 23.38	75.08	31.79	106.87
01/08/19	50.89 ± 9.24	27.97	33.55	61.52
03/15/19	45.73 ± 8.26	31.71	31.36	63.07
06/01/19	65.52 ± 13.36	47.88	41.51	89.39
Cl (mg/L)				
	Average (± Standard Deviation)	Range	Minimum	Maximum
11/21/18	473.70 ± 263.29	669.14	106.75	775.89
01/08/19	190.80 ± 27.12	70.67	141.07	211.74
03/15/19	332.20 ± 173.46	697.67	76.22	773.89
06/01/19	199.48 ± 113.97	432.84	49.91	482.75
07/26/19	191.82 ± 116.72	445.78	57.67	503.44
09/13/19	229.48 ± 136.89	522.07	57.63	579.69
11/18/19	780.14 ± 380.19	1307.52	114.46	1421.98

Table A4. Correlations among wastewater tracers, major ions, and pipe density (bold text denotes a significant *p* value for the correlation).

	OB (RFU)	B (μg/L)	Cl^- (mg/L)	Na (mg/L)	K (mg/L)	Ca (mg/L)	Mg (mg/L)	Si (mg/L)	Sanitary Pipe Density (m/km^2)	Storm Pipe Density (m/km^2)	All Pipe Density (m/km^2)
OB (RFU)	1.00										
B (μg/L)	0.28	1.00									
Cl^- (mg/L)	-0.14	0.16	1.00								
Na (mg/L)	0.03	0.28	**0.74**	1.00							
K (mg/L)	0.10	**0.40**	**0.69**	0.88	1.00						
Ca (mg/L)	0.02	0.24	**0.65**	0.89	0.82	1.00					
Mg (mg/L)	0.05	0.29	**0.74**	0.91	0.94	0.92	1.00				
Si (mg/L)	**0.23**	**0.49**	**0.32**	0.33	0.32	0.47	0.47	1.00			
Sanitary Pipe Density (m/km^2)	**-0.42**	-0.39	0.10	0.02	0.02	0.07	0.01	-0.05	1.00		
Storm Pipe Density (m/km^2)	0.10	0.09	0.15	0.08	0.10	0.03	0.03	0.00	0.10	1.00	
All Pipe Density (m/km^2)	**-0.32**	-0.33	0.15	0.05	0.06	0.07	0.03	-0.04	0.90	0.52	1.00

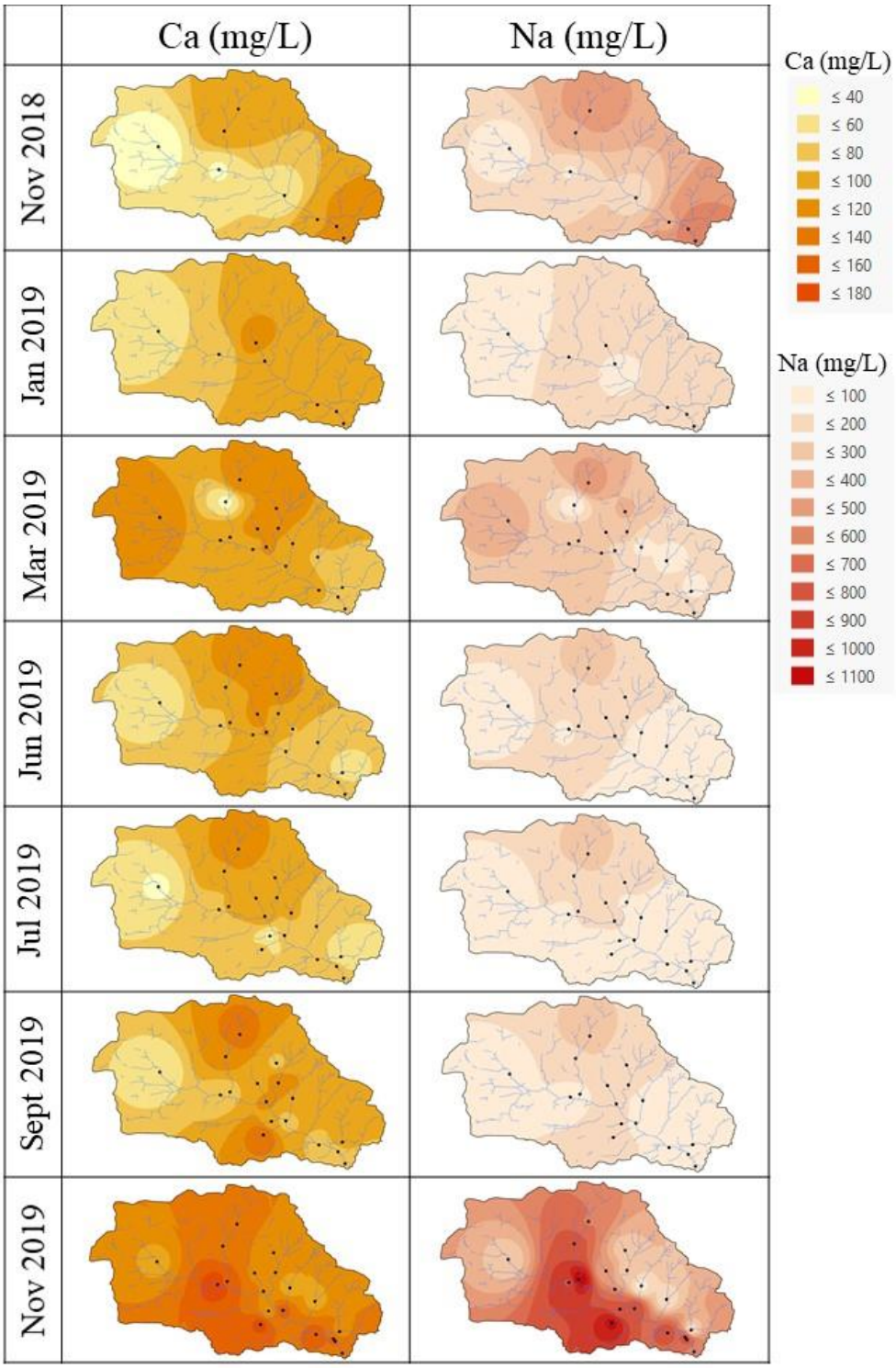

Figure A1. Spatial interpolations of Ca and Na data for each sampling event over the 1-year study period.

REFERENCES

American Society of Civil Engineers (ASCE). (2011). Failure to act: The economic impact of current investment trends in water and wastewater treatment infrastructure. Retrieved from https://www.asce.org/uploadedFiles/Issues_and_Advocacy/Our_Initiatives/Infrastructure/Content_Pieces/failure-to-act-water-wastewater-report.pdf

American Society of Civil Engineers (ASCE). (2018). Report card for Missouri's infrastructure, 2018. Retrieved from https://www.infrastructurereportcard.org/state-item/missouri/

American Society of Civil Engineers (ASCE). (2019). 2017 Infrastructure Report Card. Retrieved from https://www.infrastructurereportcard.org/cat-item/drinking_water/

Billian, H., Krometis, L., Thompson, T., & Hagerdorn, C. (2018). Movement of traditional fecal indicator bacteria and source-tracking targets through septic drainfields. *Science of The Total Environment*, 610-611, 1467-1475. https://doi.org/10.1016/j.scitotenv.2017.08.131

Cao, Y., Griffith, J. F., & Weisberg, S. B. (2009). Evaluation of OB photodecay characteristics for detection of human fecal contamination. *Water Research*, 43(8), 2273-2279. https://doi.org/10.1016/j.watres.2009.02.020

Center for Disease Control and Prevention. (CDC). (2016). Community Water Fluoridation. Retrieved from https://www.cdc.gov/fluoridation/statistics/2014stats.htm

Chetelat, B., & Gaillardet, J. (2005). Boron isotopes in the Seine River, France: A probe of anthropogenic contamination. *Environmental Science & Technology*, 39(8), 2486-2493. https://doi.org/10.1021/es048387j

Deeba, E. A. & Hasenmueller, E. A. (2018). Land use controls on groundwater inputs to streams Paper presented at the 130th Annual Meeting, Geological Society of America, Indianapolis, Indiana, USA.

Gholami, A., Masoum, S., Mohsenika, & A., Abbasi, S., (2016). Chemometrics-assisted excitation-emission fluorescence analytical data for rapid and selective dtermination of OBs in the presence of uncalibrated interferences. *Spectrochimica Acta*, 153, 108-117. https://doi.org/10.1016/j.saa.2015.08.012

Guinoiseau, D., Louvat, P., Paris, G., Chen, J. B., Chetelat, B., Rocher, V., Guerin, S., & Gaillardet, J. (2018). Are boron isotopes a reliable tracer of anthropogenic inputs to rivers over time? *Science of the Total Environment*, 626, 1057–1068. https://doi.org/10.1016/j.scitotenv.2018.01.159

Harrison, R.W., 1997, Bedrock geologic map of the St. Louis 30' × 60' Quadrangle, Missouri and Illinois: U.S. Geological Survey Miscellaneous Investigation Series Map I-2533, scale 1:100,000.

Hartel, P. G., Hagerdorn, C., McDonald, J. L., Fisher, J. A., Saluta, M. A., Dickerson, J. W., Gentit, L. C., Smith, S. L., Mantripragada, N. S., Ritter, K. J., & Belcher, C. N. (2007). Exposing water samples to ultraviolet light improves fluorometry for detecting human fecal contamination. *Water Research*, 41(16), 3629-3642. https://doi.org/10.1016/j.watres.2007.03.034

Hasenmueller, E. A. & Criss, R. E. (2013). Multiple sources of boron in urban surface waters and groundwaters. *Science of the Total Environment*, 447, 235-247. https://doi.org/10.1016/j.scitotenv.2013.01.001

Hayakawa, K., Okumura, R., Yamamoto, H., Fujiwara, M., Yamaji, N., Takeda, H., Kanematsu, & Shimizu, Y. (2007). Distribution and fluxes of fluorescent whitening agents discharged from domestic wastewater into small rivers with seasonal changes of flow rates. *Limnology*, 8(251). https://doi.org/10.1007/s10201-007-0220-6

Homer, C. G., Dewitz, J. A., Yang, L., Jin, S., Danielson, P., Xian, G., Coulston, J., Herold, N. D.,Wickham, J. D. & Megown, K. (2015). Completion of the 2011 National Land Cover Database for the conterminous United States – representing a decade of landcover change information. *Photogrammetric Engineering and Remote Sensing*, 81(5), 345-354. http://www.ingentaconnect.com/content/asprs/pers/2015/00000081/00000005/art00002

Keefe, S. H., Barber, L. E., Hubbard, L. E., Bradley, P. M., Roth, D. A., & Kolpin D. W. (2019). Behavior of major and trace elements in a transient surface water/groundwater system following removal of a long-term wastewater treatment facility source. *Science of the Total Environment*, 668(10), 867-880. https://doi.org/10.1016/j.scitotenv.2019.02.358

Lakey, B. & Krothe N. C. (1996). Stable isotopic variation of storm discharge from a perennial karst spring, Indiana. *Water Resources Research*, 32(3), 721-731. https://doi.org/10.1029/95WR01951

Lee, E. S. & Krothe, M. C. (2001). A four-component mixing model for water in a karst terrain in sourht-central Indiana, USA. Using solute concentration and stable isotopes as tracers. *Chemical Geology*, 179, 129-143. https://doi.org/10.1016/S0009-2541(01)00319-9

Lockmiller, K. A., Wang, K., Fike, D. A., Shaμghnessy, A. R. & Hasenmueller, E. A. (2019). Using multiple tracers (F-, B, s11B, and OBs) to distinguish between municipal drinking water and wastewater inputs to urban streams. *Science of the Total Environment*, 671, 1245-1256. https://doi.org/10.1016/j.scitotenv.2019.03.352

Metropolitan Sewer District (MSD), unpublished. Sewer infrastructure data. Obtained November 2018

National Oceanic and Atmospheric Administration (NOAA) (2020). Climate Data Online. https://www.ncdc.noaa.gov/cdo-web/

Passarello, M. C., Sharp, J. M. & Pierce, S. A. (2012). Estimating urban-induced artificial recharge: A case study for Austin, TX. *Environmental and Engineering Geoscience*. 18(1), 25-26. https://doi.org/10.2113/gseegeosci.18.1.25

Pfeiffer, E., Pavelescu, G., Baker, A., Roman, A., Ioja, C. & Savastru D. (2008). Pollution analysis on the Arges River using Fluorescence spectroscopy. *Journal of Optoelectronics and Advanced Materials*, 10(6), 1489-1494

Poiger 1998, T., Field, J. A., Field, T. M., Siegrist, H., & Giger, W. (1998). Behavior of fluorescent whitening agents during sewage treatment. *Water Resources*, 32, 1939-1947. https://doi.org/10.1016/S0043-1354(97)00408-9

Rugel, K., Golladay, S. W., Jackson, R., & Rasmussen, T. C. (2016). Delineating groundwater/surface water interaction in a karst watershed: Lower Flint River Basin, southwestern Georgia, USA. *Journal of hydrology: Regional Studies*, 5, 1-19. https://doi.org/10.1016/j.ejrh.2015.11.011

Stueber, A. M., & Criss, R. E. (2005). Origin and transport of dissolved chemicals in a karst watershed, Southwestern Illinois. *Journal of the American Water Resources Association*, 267-290.

Tavares, M. E., Spivery, M. I. H., McIver, M. R., & Mallin, M. A. (2008). Testing for OBs and fecal bacteria to detect sewage leaks in tidal creeks. *Journal of North Carolina Academy of Science*, 124(3), 91-97. Retrieved from https://dc.lib.unc.edu/cgi-bin/showfile.exe?CISOROOT=/jncas&CISOPTR=3904

United Nations (2018). World population prospects 2018. Retrieved from https://population.un.org/wup/publications/

United States Environmental Protection Agency (USEPA). (2018). National Pollutant Discharge Elimination System (NPDES): Municipal Wastewater. Retrieved from https://www.epa.gov/npdes/municipal-wastewater

United States Environmental Protection Agency (USEPA). (2019a). Watersense: Outdoors. Retrieved from https://www.epa.gov/watersense/outdoors

United States Environmental Protection Agency (USEPA). (2019b). The Sources and Solutions: Wastewater. Retrieved from https://www.epa.gov/nutrientpollution/sources-and-solutions-wastewater

U.S. Department of Health and Human Services Federal Panel on Community Water Fluoridation (USDH). (2015). U.S. Public Health Service Recommendation for Fluoride Concentration in Drinking Water for the Prevention of Dental Caries. (PMCID: 26346489). Retrieved from https://doi.org/ 10.1177/003335491513000408

Vengosh, A., Heumann, K. G., Juraske, S., & Kasher, R. (1994). Boron isotope application for tracing sources of contamination in groundwater. *Environmental Science & Technology*, 28(11), 1968-1974. https://doi.org/10.1021/es00060a030

Wolf, L., Held, I., Eiswirth, M., & Hötzl, H. (2004). Impact of Leaky Sewers on Groundwater Quality. *Acta hydrochimica et hydrobiological,* 32(4-5), 361-373. https://doi.org/10.1002/aheh.200400538

Wolf, L., Eiswirth, M., & Hötzl, H. (2006). Assessing sewer–groundwater interaction at the city scale based on individual sewer defects and marker species distributions. *Environmental Ge*ology, 49. 849-857. https://doi.org/10.1007/s00254-006-0180-x

World Health Organization (WHO). (1998). Boron in drinking-water. (Rep. WHO/SDE/WSH/03.04/54). Retrieved from https://www.who.int/water_sanitation_health/dwq/boron.pdf

Wyness, A. J., Parkman, R. H., & Neal, C. (2003). A summary of boron surface water quality data throughout the European Union. *Science of the Total Environment,* 314-316, 255-269. https://doi.org/10.1016.S0048-9697(03)00106-2

VITA AUCTORIS

Camille E. Buckley was awarded a Bachelor of Science (B.S.) in Environmental Science and a minor in Geology from Saint Louis University (SLU) in 2017. After her undergraduate studies, Camille worked as a lab technician in Dr. Hasenmueller's Environmental Geochemistry Lab at SLU and as a Physical Scientist intern with the USGS in Minneapolis, Minnesota. She expects to graduate from SLU in August 2020 with a Master of Science (M.S.) degree in Geoscience (Environmental Geoscience concentration). While at SLU, Camille was a teaching assistant for Earth Systems I: The Solid Earth (EAS-1010), Introduction to Environmental Science (EAS-1080), and Communicating in Science (EAS-2450). While working on her M.S. degree, Camille also served SLU's Graduate Student Association as the Vice President of External Affairs, SLU's Student Government Association as a Graduate Student Senator, SLU's College of Arts and Sciences Reorganization Task Force, and the USGS's Central Midwest Water Science Center (CMWSC) as a Volunteer for Science. Camille's M.S. research has been presented at the Geological Society of America's 2019 annual meeting in Phoenix, Arizona. After obtaining her M.S. degree, Camille will be an intern for the Geoscientists-in-the-Parks program at Hot Springs National Park, Arkansas. After her internship, she will be starting a position as a Physical Scientist with the USGS's CMWSC.